

ac Impedance Spectroscopy – A Powerful Tool For The Characterization Of Materials And Electrochemical Power Sources

P. KURZWEIL

University of Applied Sciences, Kaiser-Wilhelm-Ring 23, D-92224 Amberg, Germany.

Abstract. This presentation covers the discussion about the characterization of supercapacitors for commercial products and applications. Novel methods for the interpretation of *ac* impedance spectra are presented. Furthermore, the results of our laboratory with modified carbon electrodes, bipolar supercapacitors, fuel cells, and water electrolysis are shown.

1. Introduction

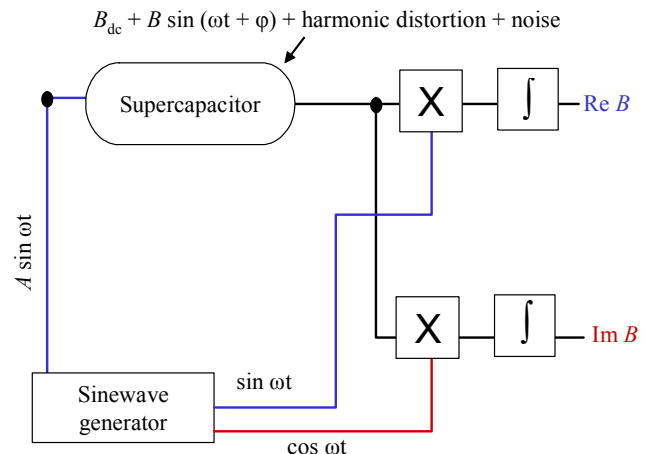
The University of Applied Sciences in Amberg is situated not far from Nuremberg in the south-west of Germany. Since 1997, manifold R & D activities have been carried out in the field of environmental engineering and energy storage. Supercapacitors for various applications in the electrotechnical, automotive and space industry are currently being developed in cooperation with HYDRA/AEG – the legal successor of the “German Edison Company for Applied Electricity” in the 19th century. Our early R & D activities on supercapacitors already began in 1991 by DORNIER (DaimlerChrysler Group) [1-9].

The **electrochemical impedance method** was developed in the 1950s, based on earlier studies of dielectric systems [10]. In the early 1980s frequency response analyzers came into the market. Meanwhile, *ac* impedance spectroscopy belongs to the routine techniques in electrochemistry [11]. By imposing potential sweeps, potential steps or current steps, the electrochemical cell is generally driven to a condition far from equilibrium, and a transient response signal is observed [12]. The *ac* impedance method perturbs the cell with an alternating signal of small magnitude. The way in which the system follows the perturbation at steady state is observed (Fig. 2). Many advantages accrue to this technique. It is capable of very high precision, because the frequency response can be averaged over a long term.

The most common experimental setup consists of a frequency response analyzer (FRA), a power source and a standard resistor R_S (Fig. 3). The sine correlation method [13] completely rejects harmonics and *dc* offsets, and noise effects are significantly reduced by the selection of appropriate integration times.



▲Fig. 1: Supercapacitor development by the University of Applied Sciences in Amberg and their partners.



▲Fig. 2: Principle of correlation analysis ($B = \sinusoidal$ response signal). There is a phase shift $\varphi = \varphi_U - \varphi_I$ between the alternating voltage U across a capacitor and the alternating current I through the capacitor. Complex impedance is given by $Z = Z e^{j\varphi}$, whereby $Z = U/I$ (rms values).

The FRA generator outputs very pure reference sine waves of given amplitudes and frequencies to the test item, and one or more analyzers to obtain magnitude and phase information about the analyzed signal. Unwanted signals are filtered out by correlating (multiplication) the return signal with the reference sine and cosine waves and integrating the results over a number of complete cycles of sines waves. The correlation result is made up of the Real (or in-phase) component, and the Imaginary (or quadrature) component.

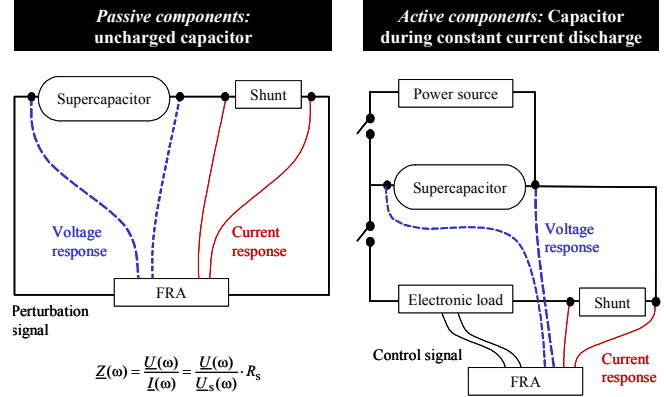
Impedance obeys Ohm's law, and equals the measured transfer function $Z(\omega) = H(\omega) \cdot R_S$ (see Fig. 3). By simple mathematical operations, it is possible to obtain the magnitude of the measured signals and the phase shift between current and voltage. In phasor notation:

$$\text{Real part, resistance: } \text{Re } Z = R = |Z| \cos \varphi$$

$$\text{Imaginary part, reactance: } \text{Im } Z = X = |Z| \sin \varphi$$

$$\text{Magnitude of impedance: } |Z| = Z = \sqrt{(\text{Re } Z)^2 + (\text{Im } Z)^2}$$

$$\text{Phase shift: } \varphi = \arctan \frac{\text{Im } Z}{\text{Re } Z}$$



▲Fig. 3: Setup for ac impedance measurements using a 2-channel-frequency response analyzer.

a) *Potentiostatic measurement* (left): The sinusoidal excitation voltage is generated by a frequency response analyzer and applied directly or over a potentiostat to the capacitor. The potentiostat controls a constant voltage across the capacitor, and transforms the current through the capacitor into a voltage which is returned to the frequency response analyzer.

b) *Galvanostatic measurement* (right): An electronic load (current sink) is controlled by the frequency response analyzer. Impedance is measured during the constant current discharge of the supercapacitor.

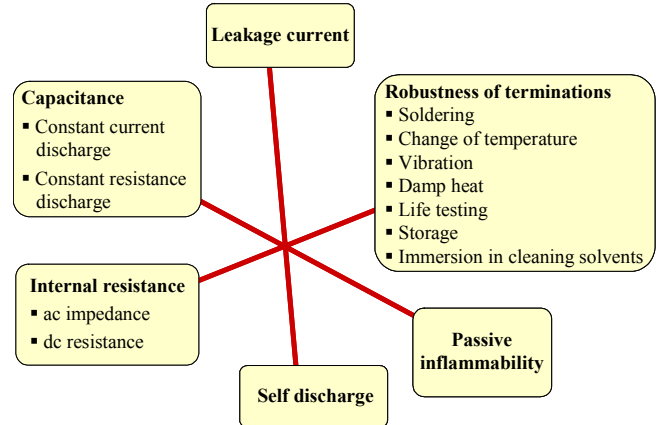
2. IEC Standards

IEC 40/1378 and the German translation DIN IEC 62391 [14,15] create a draft international standard of supercapacitors for use in electronic equipment and power applications. Essential parts of environmental testing refer to IEC 60068, which is valid for conventional capacitors. Correspondingly, electrical tests have to be performed at temperatures between 15 °C and 35 °C, a relative humidity of 45 % to 75 %, and an atmospheric pressure of 86 to 106 kPa. Reference conditions are 20 °C, and 101.3 kPa.

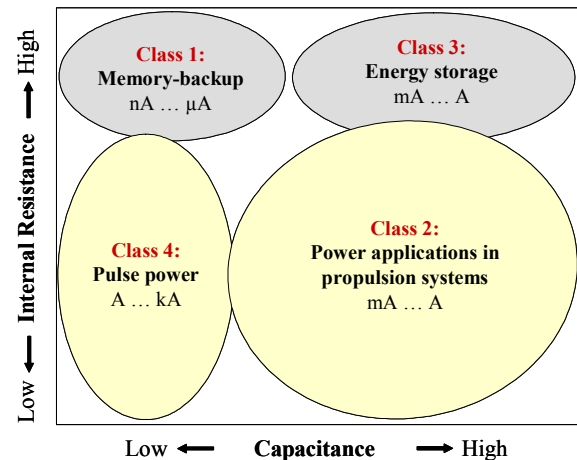
In an circulating air oven, the capacitor has to be dried for (96 ± 4) hours at (55 ± 2) °C, and a relative humidity of not more than 20 %. In a dehydrator using an appropriate desiccant such als Al_2O_3 or silica, the capacitor may cool off, and rest until it is needed for testing.

In a *sight check*, the dimensions of the capacitor, and the correct labelling according to the design specification are verified. Materials, design, dimensions, fabrication processes, and rated values according to the specification are checked.

A certain number of capacitors is tested according to a standardized schedule, and after each step examined under a microscope at 10-fold magnification. Any visible damages or losses of electrolyte are not allowed. A capacitor for power applications must not lose more than 10 % to 30 % of its rated capacitance during the mechanical and electrical test procedures.



▲Fig. 4: Testing of supercapacitors (DIN IEC 62391)



▲Fig. 5: Classification of supercapacitors (DIN IEC 62391)

Capacitance is determined by *constant current discharge* according to Fig. 6. The supercapacitor is charged at its rated *dc* voltage for 30 minutes, as far as different values are not specified elsewhere. Then, the power source is electrically cut off, and the constant current discharge appliance (e. g. an electronic load) is switched on. The period of time $t_2 - t_1$ is measured, during which the voltage across the capacitor declines from 80 % to 40 % of the applied voltage E .

$$C = \frac{\Delta Q}{\Delta U_C} = \frac{I \cdot (t_2 - t_1)}{U_1 - U_2} \quad (1)$$

If the voltage drop due to the internal resistance exceeds a limit of 5 % of the applied voltage ($IR \geq 0.05 E$), the discharge current according to Table 1 may be reduced by a factor of two, a fifth or a tenth. Current values $I > 10$ A are rounded to two significant digits and currents $I \leq 10$ A to one significant digit respectively.

Internal resistance. The steep descent (*IR drop*) in the constant current discharge curve provides the ohmic *dc* resistance of the capacitor (see Fig. 7 left). According to DIN IEC 62391-1 the voltage drop $\Delta U_R = IR$ is determined as the point of intersection between the linearly extrapolated voltage curve and the time axis immediately after closing the discharge circuit.

$$R = \frac{\Delta U_R}{I} \quad (2)$$

If the voltage drop exceeds 20 % of the applied voltage ($\Delta U_R \geq 0.2 E$), the discharge current according to Table 1 may be reduced by the half, a fifth or a tenth.

Electric power reflects the maximum current the supercapacitor is able to supply, when it is discharged to the half of its rated voltage. DIN IEC 62391-1 reads:

$$P = \frac{(U_1 + U_2) \cdot I}{2} = \frac{(0.6 \cdot E) \cdot \Delta U_R}{R} \approx \frac{0.12 \cdot E^2}{R} \quad (3)$$

The latter approximation is valid only if the voltage drop equals $\Delta U_R = E - U_1 = 0.2 E$ (see Figs. 6/7 left). With this, *specific power* $P_m = P/m$ (in W/kg, m = mass of the capacitor), and *power density* $P_V = P/V$ (in W/l, V = volume of the capacitor) can be calculated.

▼Table 1: Constant current discharge (DIN IEC 62391)

	Classification of supercapacitors (see Fig. 5)			
	Class 1	Class 2	Class 3	Class 4
a) Measurement of capacitance				
I (mA) · Δt	1 V · C	4·CU	0.4·CU	400·CU
b) Measurement of internal resistance				
I (mA) · Δt	10 V · C	40·CU	4·CU	400·CU
U_1	80 % of the charging voltage ($0.8 \cdot E$)			
U_2	40 % of the charging voltage ($0.4 \cdot E$)			

C rated capacitance of the supercapacitor

CU electric charge: product of rated capacitance and rated voltage

The **ac resistance** or *equivalent series resistance* (ESR) reflects directly the ohmic losses of the supercapacitor. R_i is determined as the real part of impedance at a high frequency. A good approximation is the ratio of rms voltage and rms current (1 mA ... 10 mA) at 1 kHz.

$$R_i \approx Z(1 \text{ kHz}) = \frac{U_{\text{rms}}}{I_{\text{rms}}} \quad (4)$$

The *ac* method is normative for capacitors working at low currents (Class 1). For power applications, DIN IEC 62391-2 specifies that the internal resistance of supercapacitors *may* be measured using the constant current discharge method (equation 2) even if the *ac* resistance is available likewise.

Charging at constant voltage (Fig. 6 right) requires a regulated power supply. The current-limiting series resistor $R_S \leq 1000 \Omega$ is so chosen that the time constant $\tau = R_S C$ equals 60 to 120 s. A design specification may ordain something different. Before the measurement, the capacitor terminations are short-circuited for at least 30 minutes. τ is determined as the time until the voltage across the capacitor reaches 63.2 % of the applied voltage ($0.632 E$). The small internal resistance of the supercapacitor is neglected ($R_i \ll R_S$).

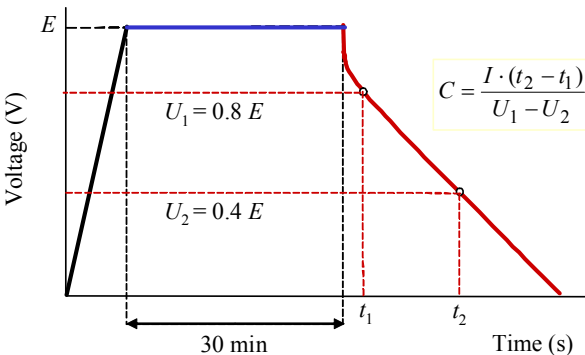
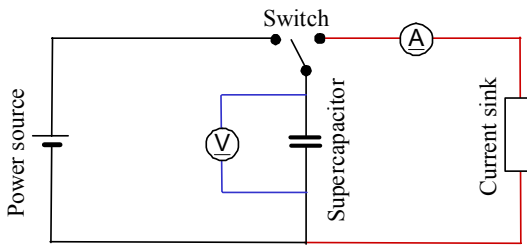
$$C = \frac{\tau}{R_i + R_S} \approx \frac{\tau}{R_S} \quad (5)$$

The **leakage current** is flowing when the capacitor is fully charged after at least 30 minutes, and the voltage across the capacitor reaches the applied voltage E . The leakage current is defined at a reference temperature of 20 °C. A regulated power supply and a protective series resistance $R_S \leq 1000 \Omega$ are used. The error of measurement must be lower than ± 5 % (or 0,1 μA).

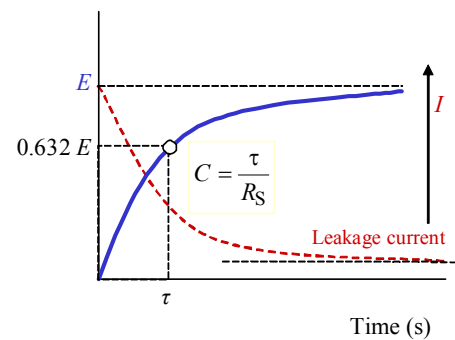
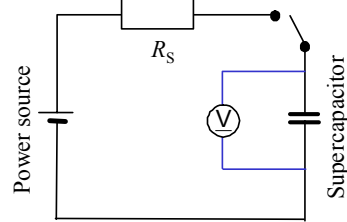
Self discharge is measured at the fully charged capacitor. After a constant current charge over 8 or 24 hours without a protective resistance, the terminals are disconnected. After a rest period of 24 hours, the voltage across the capacitor is measured using a *dc* voltmeter with an internal resistance of at least 1 MΩ. Supercapacitors for power applications must show a retention voltage of > 80 % of the charging voltage after 24 hours of charging and 24 hours of resting.

Figure 8 summarizes some electrical and mechanical requirements, supercapacitors for power applications have to meet. In the **aging test** at constant voltage, the supercapacitor is charged at a test voltage higher than the rated voltage, and at an ambient temperature of 60 °C or 70 °C for 2000 hrs or 1000 hrs respectively. The relative decrease of capacitance and the increase of resistance after the test reflect the quality of the supercapacitor.

Constant current discharge

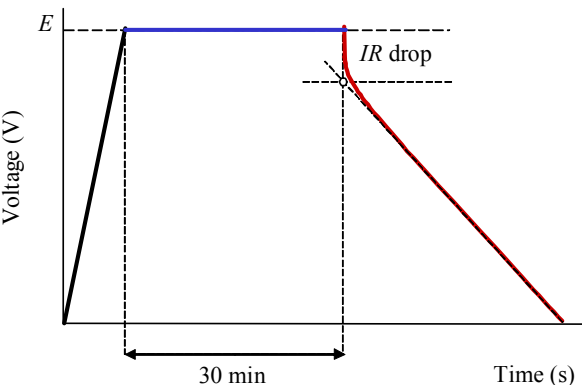


Charging at constant voltage



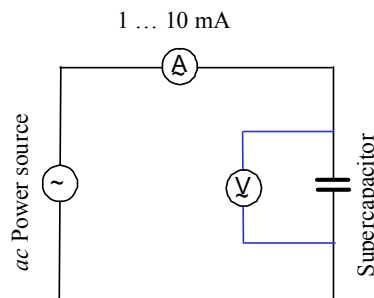
►Fig. 6

Constant current discharge



Point of intersection between begin of discharge and extrapolated voltage characteristics

ac Impedance measurement



Magnitude of impedance at 1 kHz

$$R_i = Z(1 \text{ kHz}) = \frac{U_{\text{rms}}}{I_{\text{rms}}}$$

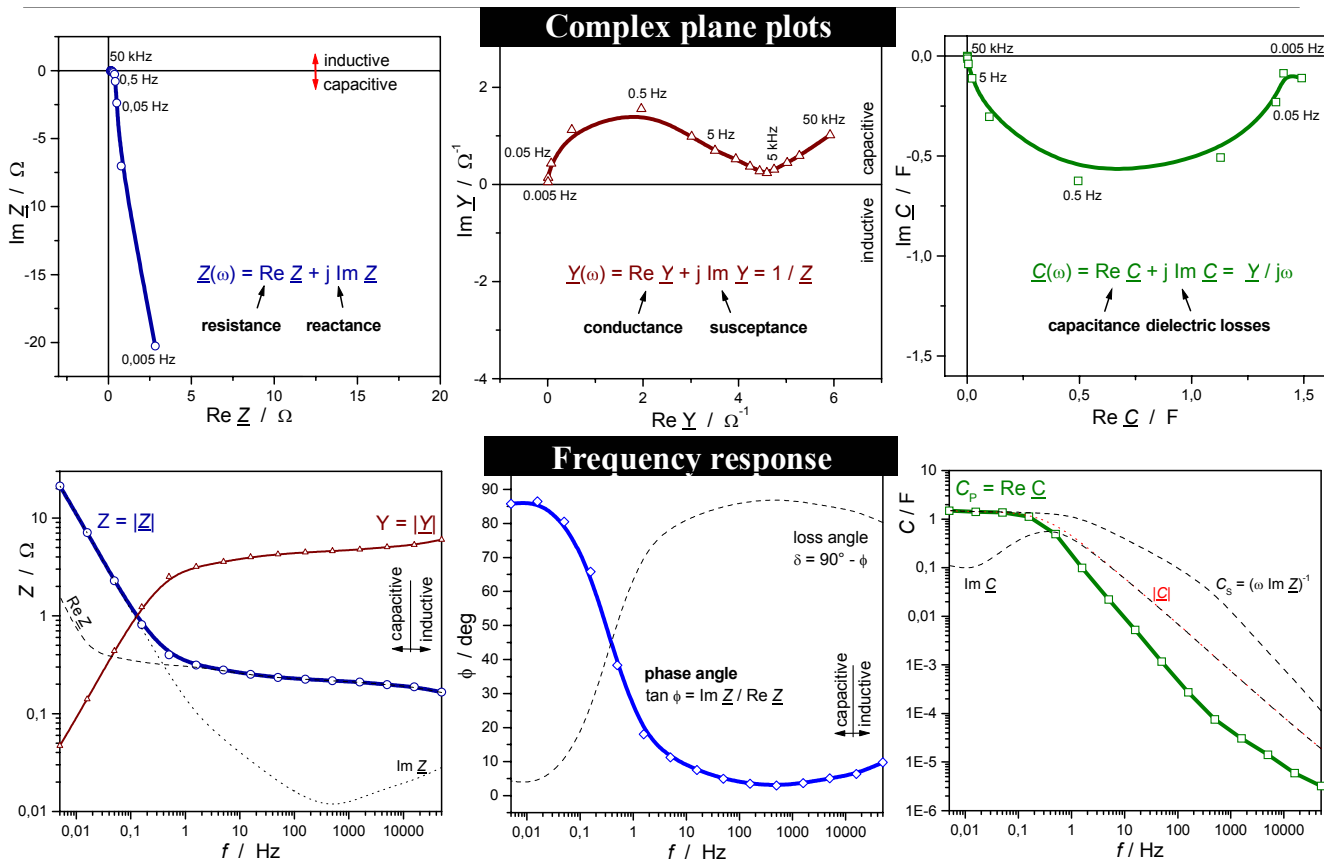
Classes 2 to 4: normative for high-current capacitors

Class 1: normative for low-current capacitors

►Fig. 7

Testing schedule	0	Sight check Leakage current at 20 °C Capacitance Internal dc resistance	Materials, design, dimensions, fabrication, rated values (C, R) according to the specification	56 + 2 samples	Destructive: every 6 months (1 & 4 every year) 0 nonconforming samples allowed!
	1A	Robustness of terminations Soldering heat stability	No visible damage, no loss of electrolyte, and $\Delta C/C \leq 10\%$ after each step: tensile load, bending load, soldering iron or bath, five temperature cycles, vibration (6 h at 10...55 Hz, 100 m/s ²)	8	
	1B	Solderability Change of temperature Vibration		8	
	2	Aging test at constant proof voltage	No visible damage, no loss of electrolyte, $\Delta C/C \leq 30\%$, $\Delta R/R \leq 4$ after 70 °C/1000 h or 60 °C/2000 h	16	
	3A	Self discharge Storage at high temperature	Voltage loss < 20 % after 24 h. $\Delta C/C \leq 10\%$, $\Delta R/R \leq 2$ after (96+4) h	8	
	3B	Damp heat (40 °C, 90...95 %)	$\Delta C/C \leq 30\%$, $\Delta R/R \leq 4$ after 10 days	8	
	4	Jump in temperature: $20^{\circ}\text{C} \rightarrow T_1 \rightarrow T_2$	$\Delta C/C \leq 30\%$, $\Delta R/R \leq 4$ after step 1 $\Delta C/C_1 \leq 30\%$, $\Delta R/R \leq 1$ after step 2	8	

▲ Fig. 8.: Test schedule for supercapacitors for power applications (DIN IEC 62391-2).



▲ Fig. 9: Diagram types: impedance spectra of a series combination of eight supercapacitors (Panasonic 10 F / 2,5 V). Note the mathematical convention of impedance, which shows capacitive reactance on the negative imaginary axis.

3. Frequency Response of Capacitance And a Novel Diagram Type

3.1 Definitions of capacitance relevant to practice

The general equivalent circuit of a technical capacitor (Fig. 10) comprises the utilizable capacitance C_p , the *dc* isolation resistance R_p , the series resistance R_s and capacitance C_s of the electrolyte space (including contact resistances), an inductance L (taking account of cables, leads, and spiral wound electrodes), and unwanted stray capacitances due to casing and grounding. In highly conductive solutions R_s is small, and C_s is negligible. Only with membrane electrolytes or weakly conducting interlayers between electrodes and current connector, R_s and C_s cause a distinct semi-circle in the complex plane plot at high frequencies. Neglecting stray capacitances, the utilizable capacitance of a supercapacitor reads:

$$C_p(\omega) = \frac{-(\text{Im} Z - \omega L)}{\omega \cdot [(\text{Re} Z - R_s)^2 + (\text{Im} Z - \omega L)^2]} \quad (6)$$

The informative Appendix B of DIN IEC 62391-1 recommends an easy-to-use *ac* impedance method for the determination of *capacitances*, which fits for supercapacitors with low resistance and low capacitance (Class 4). Simplified, the supercapacitor is modelled by a RC series combination of a resistance R_s and a capacitance C_s . This *equivalent series capacitance* C_s is given by the reciprocal of reactance (the imaginary part $\text{Im} Z$ of impedance) multiplied by the

circular frequency $\omega = 2\pi f$. The measuring frequency f shall be low (see Fig. 10 C)

$$\text{Im } Z = |\underline{Z}| \sin \varphi \Rightarrow C_s = \frac{-1}{2\pi f \cdot \text{Im} Z} \quad (7)$$

Equation (7) implies that the *dc* resistance R_p of the capacitor is infinitely high. This is mostly not valid in practice, as supercapacitors show considerable leakage currents and self discharge. At high frequencies, C_s depicts the supercapacitor better than it really is.

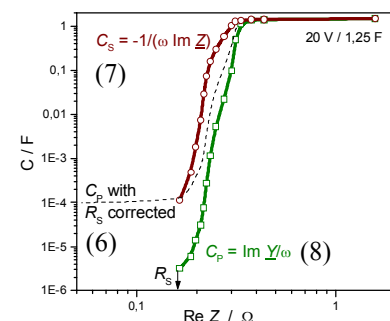
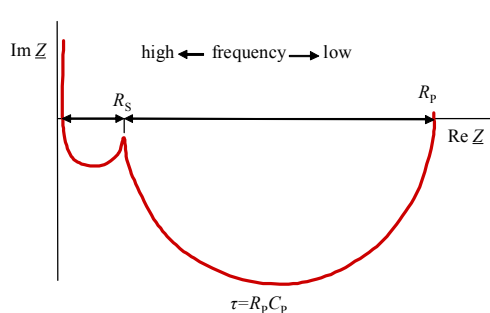
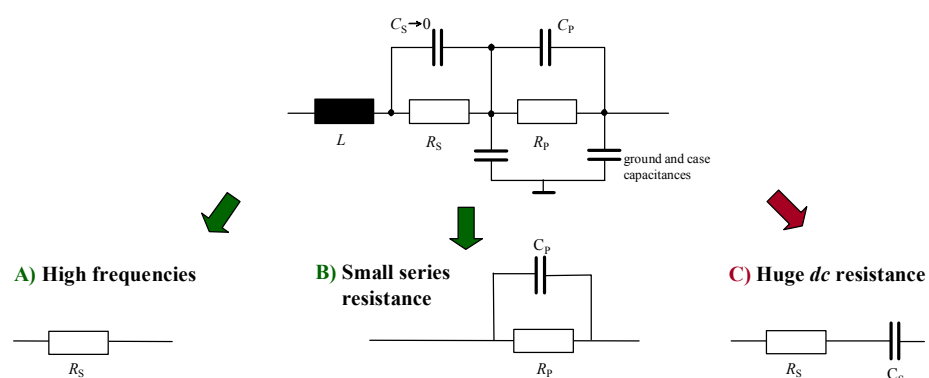
For supercapacitors with high capacitance and low internal resistance R_s , we suggest to evaluate the *equivalent parallel capacitance* (see Fig. 10 B).

$$C_p(\omega) = \frac{\text{Im} Y}{\omega} = \frac{-\text{Im} Z}{\omega \cdot |\underline{Z}|^2} = \frac{-\text{Im} Z}{\omega \cdot [(\text{Re} Z)^2 + (\text{Im} Z)^2]} \quad (8)$$

Equation (8) follows from (6) for $R_s \rightarrow 0$ and $L \rightarrow 0$. In advanced supercapacitors, R_s equals less than a Milliohm, so that C_p reflects directly the utilizable capacitance. Inductances L up to some Microhenrys in spiral wound devices can be neglected in view of several thousand Farads of capacitance. At low frequencies, series and parallel capacitance coincide.

We propose the diagram of capacitance versus resistance as a novel representation to depict the performance data of supercapacitors.

Figure 10 shows the capacitances calculated according to equations (6), (7), and (8) for a series combination of eight supercapacitors. The useful capacitance and the internal resistance R_s (ESR) can directly be read. Further applications of the diagram are shown below.



► Fig.10

▼ Table 2: Definition of *ac* power quantities. Complex quantities are written with an underline to differ them from magnitudes (apparent values). Conjugated complex quantities are marked with a star. Examples see Figure 9.

	Complex quantity	Real part	Imaginary part	Apparent value
Impedance	$Z(\omega) = \text{Re } Z + j \text{Im } Z$	$R = \text{Re } \underline{Z}$	$X = \text{Im } \underline{Z}$	$Z = \underline{Z} = \sqrt{(\text{Re } \underline{Z})^2 + (\text{Im } \underline{Z})^2} = \frac{U}{I}$
Admittance	$\underline{Y}(\omega) = \text{Re } \underline{Y} + j \text{Im } \underline{Y} = \frac{1}{\underline{Z}(\omega)}$	$G = \frac{\text{Re } \underline{Z}}{ \underline{Z} ^2}$	$B = -\frac{\text{Im } \underline{Z}}{ \underline{Z} ^2}$	$Y = \underline{Y} = \sqrt{(\text{Re } \underline{Y})^2 + (\text{Im } \underline{Y})^2} = \frac{1}{Z}$
Capacitance	$\underline{C}(\omega) = \text{Re } \underline{C} + j \text{Im } \underline{C} = \frac{Y}{j\omega}$	$C_p = \frac{\text{Im } \underline{Y}}{\omega}$	$\sigma = -\frac{\text{Re } \underline{Y}}{\omega}$	$C = \underline{C} = \sqrt{(\text{Re } \underline{C})^2 + (\text{Im } \underline{C})^2} = \frac{Y}{\omega}$
Power	$\underline{S} = \underline{U} \underline{I}^* = U^2 \underline{Y}^* = -j\omega U^2 \underline{C}^*$	$P = U^2 \text{Re } \underline{Y}$	$Q = -U^2 \text{Im } \underline{Y}$	$S = \underline{S} = \sqrt{(\text{Re } \underline{S})^2 + (\text{Im } \underline{S})^2} = U^2 Y$
Phase angle		$\text{Re } \underline{A} = \underline{A} \cos \varphi$	$\text{Im } \underline{A} = \underline{A} \sin \varphi$	$\tan \varphi = \frac{\text{Im } \underline{Z}}{\text{Re } \underline{Z}}$

U rms voltage, I rms current, \underline{A} any complex quantity (except \underline{C} : replace φ by δ here), $\omega = 2\pi f$ circular frequency.
 R resistance, X reactance, G conductance, C_p capacitance.

3.2 A more general idea of capacitance

The complex plane plot of impedance mostly shows a depression of the semicircles – which cannot easily be modelled by the general equivalent circuit in Figure 10. Therefore, we try to derive capacitance $C_p(\omega)$ from the electrotechnical definitions of *ac* power quantities, which require no model assumptions (Table 2).

A plate capacitor filled with a homogeneous dielectric can be described by a *complex permittivity* $\underline{\epsilon} = \text{Re } \underline{\epsilon} + j \text{Im } \underline{\epsilon}$. Its real part describes the ratio of the complex amplitudes of electric flux density (displacement \underline{D}) and field strength \underline{E} . The imaginary part comprises all dielectric losses due to the conductivity σ of the medium. The loss factor in a dielectric can be measured by impedance spectroscopy.

$$\underline{\epsilon} = \text{Re } \underline{\epsilon} + j \text{Im } \underline{\epsilon} \Leftrightarrow \tan \delta = \frac{\text{Im } \underline{\epsilon}}{\text{Re } \underline{\epsilon}} = \frac{\text{Re } \underline{Y}}{\text{Im } \underline{Y}} \quad (9)$$

With permittivity $\underline{\epsilon}$ being a complex quantity, the capacitance of a supercapacitor can be expressed in complex notation, too.

$$\underline{C} = \epsilon_0 \underline{\epsilon} \frac{A}{d} = C_0 \underline{\epsilon}_r = \text{Re } \underline{C} + j \text{Im } \underline{C} \quad (10)$$

Equation 8' represents the real part $C_p = \text{Re } \underline{C}$, and is directly related to the reactive power of the supercapacitor. The imaginary part $\text{Im } \underline{C}$ comprises all dielectric losses. Equivalent series and parallel capacitance (see Fig. 10) read by help of the loss angle δ .

$$C_p = \text{Re } \underline{C} = \frac{Y \cos \delta}{\omega} \quad (8')$$

$$\text{Im } \underline{C} = -C_p \tan \delta \quad (11)$$

$$C_s = \frac{Y}{\omega \cos \delta} = \frac{1}{\omega^2 Z^2 C_p} \quad (12)$$

3.3. Estimation of energy and power densities

a) The *maximum dc power* is mostly determined under short-circuit conditions. If the outer discharge resistance R_a equals the internal ohmic resistance $R_i = \text{Re } \underline{Z}$ of the power source, the maximum *dc* power flows when $x = 50\%$ of the open circuit voltage U_0 is reached. U_0 denotes the charging *dc* voltage applied to the capacitor.

$$P = UI = \frac{U x U_0}{R_i} = \frac{(1-x)x U_0^2}{R_i}, \text{ and } \frac{dP}{dx} = 0 \text{ for } x = \frac{1}{2}$$

$$\Rightarrow P_{\max} = \frac{U_0^2}{4R_i} = \frac{1}{2} U_0 I \quad (13)$$

In the impedance spectrum, R_i is found by extrapolation at *high-frequencies*. In other words, P_{\max} is obtained by one fourth of the active power $U_0^2 \text{Re } \underline{Y}$ at high frequencies (see Figure 11).

b) As a different approach, we propose to read the maximum reactive power $Q = -U_0^2 \text{Im } \underline{Y} = U_0^2 \omega C_p$ in the impedance spectrum (see Figure 11).

This assumption seems to be justified, because supercapacitors can be modelled by an equivalent circuit consisting of linear network elements (such as R_S , R_P and C_p with constant values). In this case, the small signal behaviour measured by *ac* impedance describes the supercapacitor completely. According to TELLEGREN's theorem with BRUNE's pseudo functions, total power comprises the sum of all active power consumers (resistors) and reactive power sources (capacitors) in the network [16].

$$\underline{S} = \underline{P} + j \underline{Q} \quad (14)$$

$$\underline{U} \underline{I}^* = \sum_i R_i |I_i(j\omega)|^2 + \sum_k \frac{1}{j\omega C_k} |I_k(j\omega)|^2$$

For a network $R_S - C \parallel R_P$, apparent power reads:

$$\underline{S} = R_S |\underline{I}(j\omega)|^2 + R_P |\underline{I}_P(j\omega)|^2 + \frac{1}{j\omega C} |\underline{I}_C(j\omega)|^2 \\ = |\underline{I}(j\omega)|^2 \cdot \text{Re } \underline{Z} + j |\underline{I}(j\omega)|^2 \cdot \text{Im } \underline{Z}$$

By help of $Z = U/I$, and $\text{Im } \underline{Y} = -\text{Im } \underline{Z}/Z$, apparent power reads:

$$\underline{S} = |\underline{U}(j\omega)|^2 \cdot \text{Re } \underline{Y} - j |\underline{U}(j\omega)|^2 \cdot \text{Im } \underline{Y}$$

For a given charging *dc* voltage, the measured admittance provides the maximum power of the capacitor.

$$P = U_0^2 \cdot \text{Re } \underline{Y} \quad (15)$$

$$Q = -U_0^2 \cdot \text{Im } \underline{Y} = U_0^2 \omega C_P \quad (16)$$

c) The *energy content* of the capacitor can be calculated using *dc* capacitance at *low-frequencies*. An example is shown in Figure 11.

$$W = \int_0^{U_0} UC \, dU = \frac{1}{2} CU_0^2 \quad (17)$$

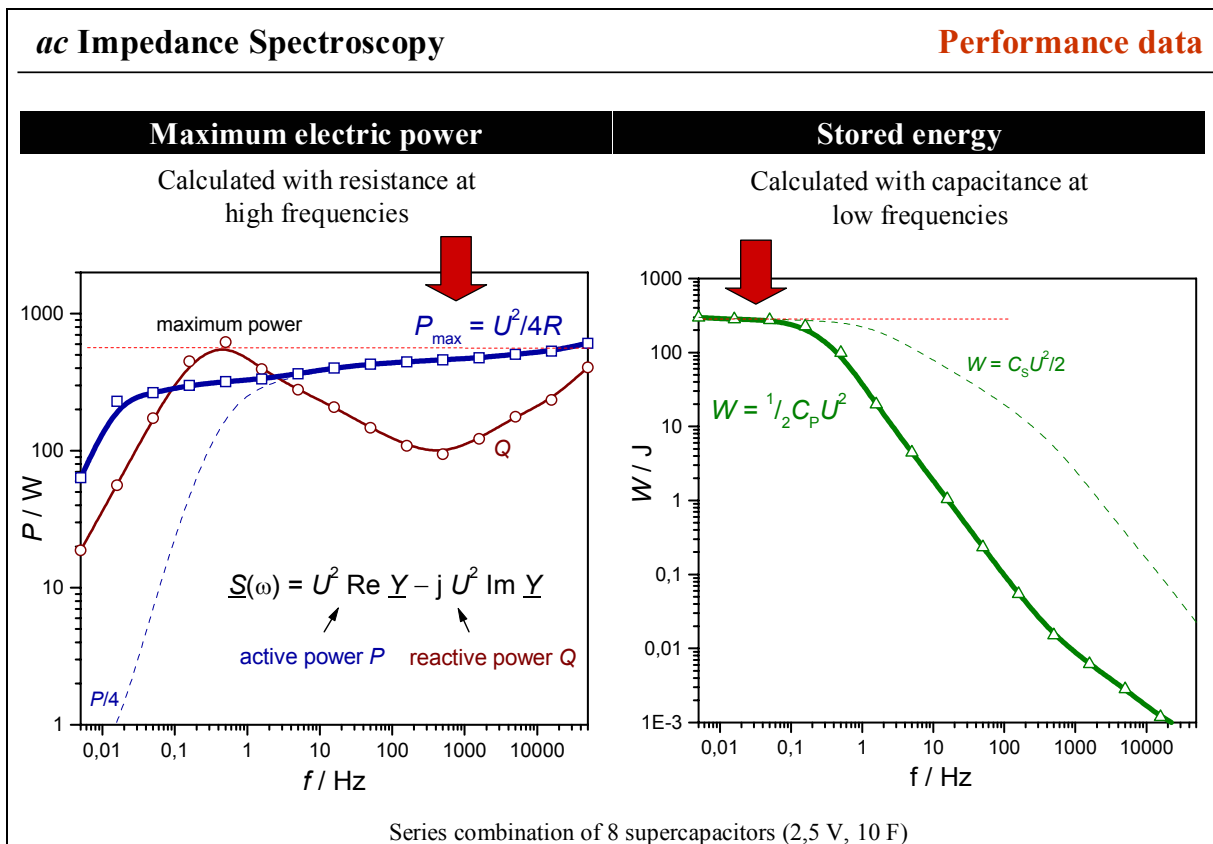
3.4. Practical benefit of the $C(R)$ diagram

The diagram of $R = \text{Re } \underline{Z}$ versus $C = \text{Im } \underline{Y}/\omega$ (equation 8) provides an easy access to the rated data of a supercapacitor, such as capacitance, ESR, energy and power densities [17,18]. The diagram in Figure 12 presents the performance data more clearly than the complex plane or BODE plot. Electively, a logarithmic C axis facilitates the extrapolation of the *equivalent series resistance* R_S (ESR) and *dc* capacitance C_P . Capacitance according to

equation (7) changes its sign at a certain high frequency from positive (capacitive behaviour) to negative (inductive behaviour, for example in spiral wound devices). On the $\log |C_P|$ scale a minimum occurs. Thus, ESR, rated capacitance, and the transition to inductive behaviour at high frequencies are obvious in a single diagram.

Different from the impedance imaginary parts in the complex plane, capacitances can be interpreted as a measure for electrode activity, surface coverage, and the state-of-charge of an energy store. The frequency response of capacitance reflects the amount of surface area accessible to the electrolyte. Capacitance at high frequencies shows the *outer* electrode surface, which may depend on grain boundaries and other interparticle phenomena. Capacitance at low frequencies shows the *inner* electrode surface, which is primarily determined by the pore size distribution and the speed of ion transport through the porous electrode. This way, the analysis of the $C-R$ -diagram supports the characterisation of new materials and the monitoring of supercapacitors in practical applications.

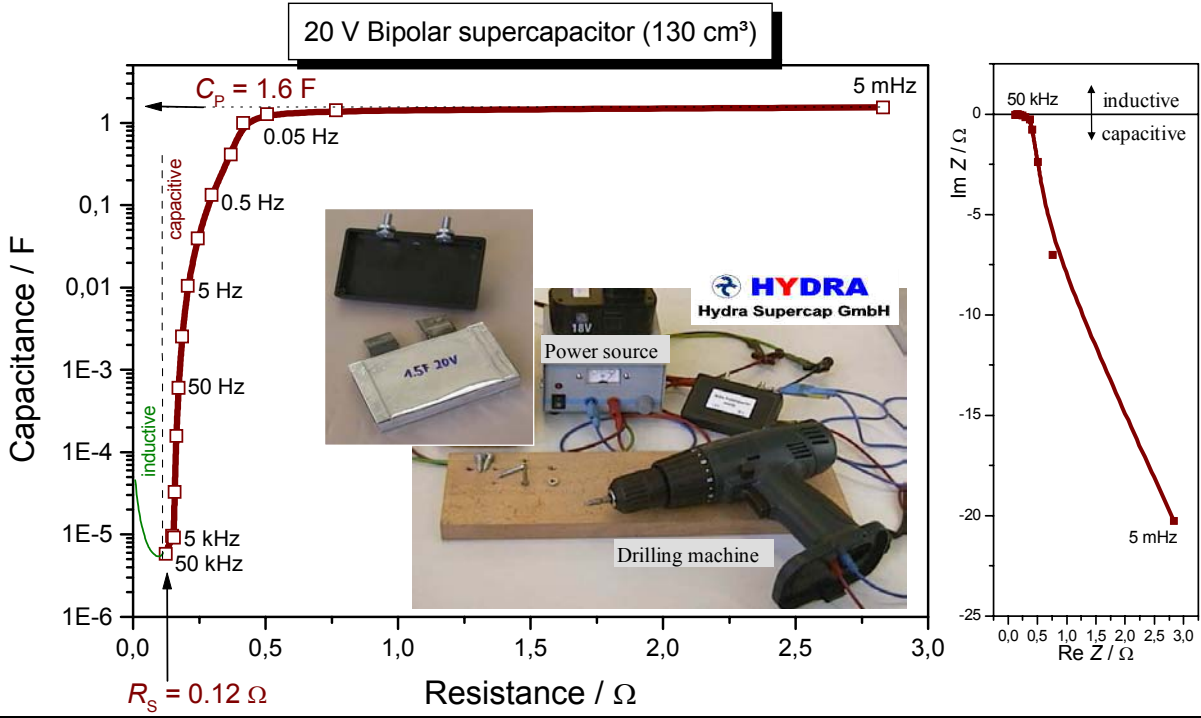
Figure 13 shows the impedance spectrum of a fuel cell operated at a constant current of $0,1 \text{ A/cm}^2$. In the $C-R$ -diagram, capacitance calculated according to equation (8) is further evaluated by separation in the individual capacitances of the solid electrolyte, the charge transfer reaction, and the limiting mass transport.



▲ Fig. 11

ac Impedance Spectroscopy

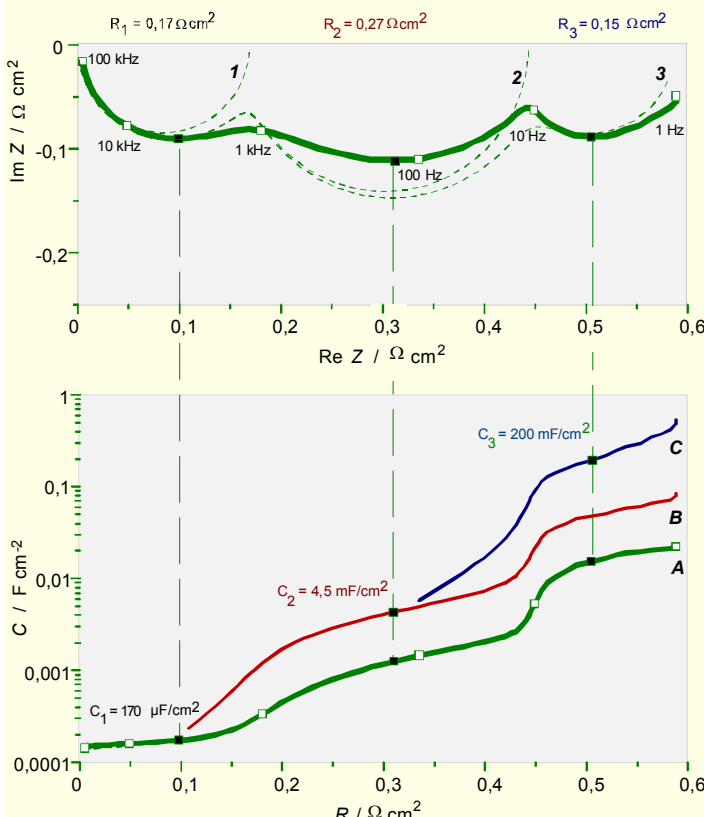
A novel diagram type: *C* versus *R*



▲Fig.12

ac Impedance Spectroscopy

Applications: PEM Fuel Cell



▲Fig.13

Impedance at 100 mA/cm²

1 Membrane arc

2 Electrode arc

3 Mass transport arc

A Measured capacitance
 $C = \text{Im } Y / \omega$

B Membrane arc **1** corrected
 $X_i(\omega) := \text{Im } Z_i - \text{Im } Z_{1,\infty}$

$R_i(\omega) := \text{Re } Z_i - R_1$

$C_i(\omega) := -X_i / [\omega (R_i^2 + X_i^2)]$

C Electrode arc **2** corrected

4. Applied Impedance Spectroscopy

4.1 ac Impedance versus transient techniques

The easy-to-use constant voltage method in [Figure 6](#) according to DIN IEC 62391 provides a more or less correct estimation of the actual capacitance of a supercapacitor. Exact measurements require to integrate the current flowing through the capacitor with respect to time. This procedure consumes considerable effort, and the correction of leakage currents I_0 forms an unwanted source of error.

$$C = \frac{Q}{\Delta U} \quad \text{wherein} \quad Q = \int [I(t) - I_0] dt \quad (13)$$

The *ac* impedance method provides capacitances in much shorter time. Leakage currents play no role, as the frequency response analyser discards the *dc* components.

The state-of-charge of the supercapacitor is obtained as the ratio of the *dc* capacitance and the measured capacitance at any time at a low frequency (for example 1 Hz or 0,1 Hz).

$$\alpha = \frac{Q(U)}{Q(U_0)} = \frac{C(U)}{C(U_0)} \quad (14)$$

A Solartron 1250 frequency response analyser was used to record the impedance spectra of a commercial supercapacitor at different applied voltages. As shown in [Figure 13](#), both capacitance and stored energy depend on voltage. For the applied voltages between 0.75 and 2.5 V, electric charge was evaluated by numerical integration of the measured discharge current with respect to time. The results strongly depend on the correction of the leakage current ([Table in Figure 13](#)).

The impedance measurement provides directly the capacitances and the state-of-charge values without need for determining leakage currents and other mathematical efforts. α equals 87 %, 94 %, 97 %, 100 % at 0.75, 1.4, 1.8 and 2.5 V respectively.

Thus, impedance spectroscopy qualifies for routine measurements of capacity and state-of-charge of supercapacitors.

4.2 ac Impedance versus RAGONE plot

[Figure 14](#) shows that energy and power calculated from the *ac* impedance spectrum lie correctly in the range of values which are obtained by the current discharge method. For the latter method, energy was determined by integration of the measured discharge power with respect to time.

$$W = \int U(t) I(t) dt \quad (15)$$

Peak power was determined in the $P(t)$ transient.

The upper limit of the gray area depicts the maximum possible power and energy which derive from the applied voltage $U = 18$ V, and the constant current flowing through the capacitor during the discharge time Δt .

As a result, the impedance method provides valuable values of energy and power in the correct order of magnitude, which normally are measured laboriously by transient techniques.

4.3 Impedance of porous electrodes

Nearby every electrochemical system shows an impedance spectrum in the complex plane which consists of three regions. Simply speaking, every phase boundary causes its own arc in the complex plane.

- The high frequent arc characterizes the electrolyte. In highly conducting solutions only the point of intersection with the real axis is visible and called the electrolyte resistance R_{el} . In thick layers of powder electrodes, a quarter circle is observed which is due to the grain boundaries. [Figure 14](#) shows active carbon electrodes, [Figure 16](#) ruthenium dioxide on nickel.
- Impedance at medium frequencies reflects the electrode reactions, especially the charge transfer at the electrode/electrolyte interface. Capacitance $C_p(\omega)$ approaches the value of the double layer capacitance at very high frequencies [19]. See Figure 10 No. 6.
- The low frequent arc mostly shows the influence of mass transport, related to the microporous structure of the interface between electrode and electrolyte.

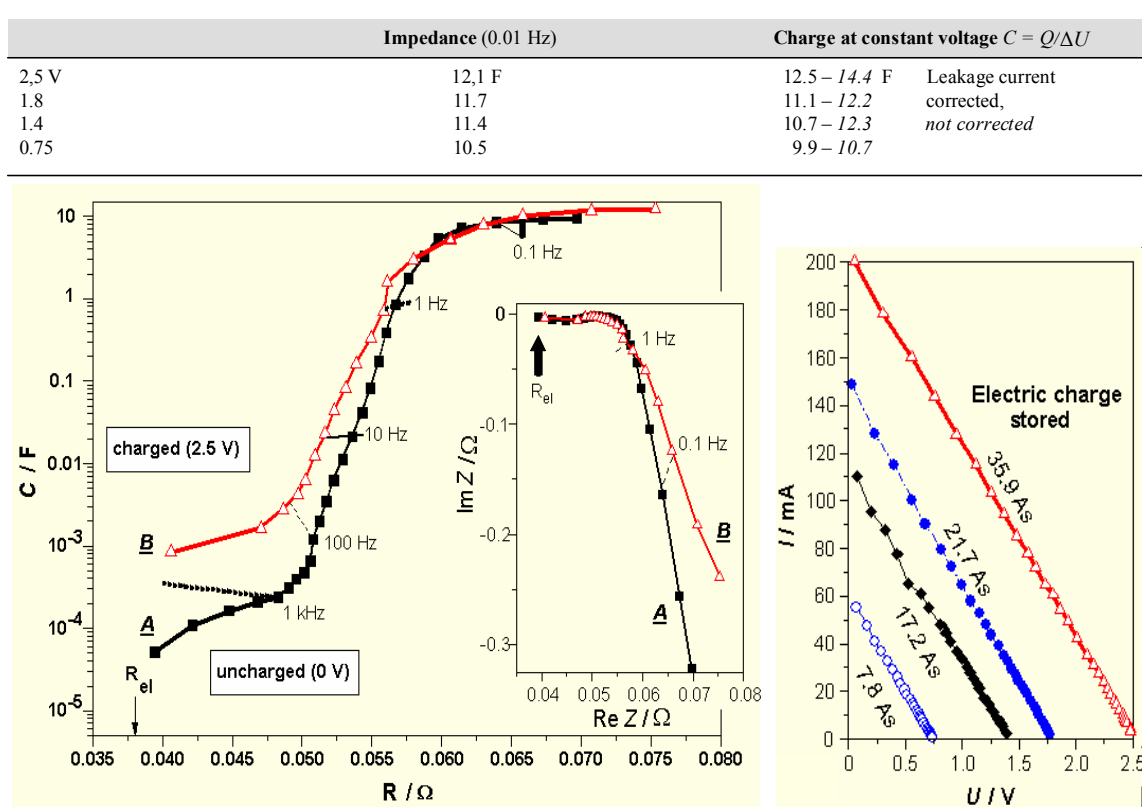
The complex plane plot of a porous supercapacitor electrode can be explained by help of the DE LEVIE model [20]. The current flow $I = C v$ through the electrode depends on the double-layer pseudocapacitance C and the voltage gradient v , and the faradic current due to the electrode reactions (I_f). It is limited by the voltage drop in the pore system. The impedance of a one-dimensional pore of the length l is given by:

$$Z(i\omega) = \frac{a \coth \sqrt{l^2 b}}{\sqrt{b}} \quad (16)$$

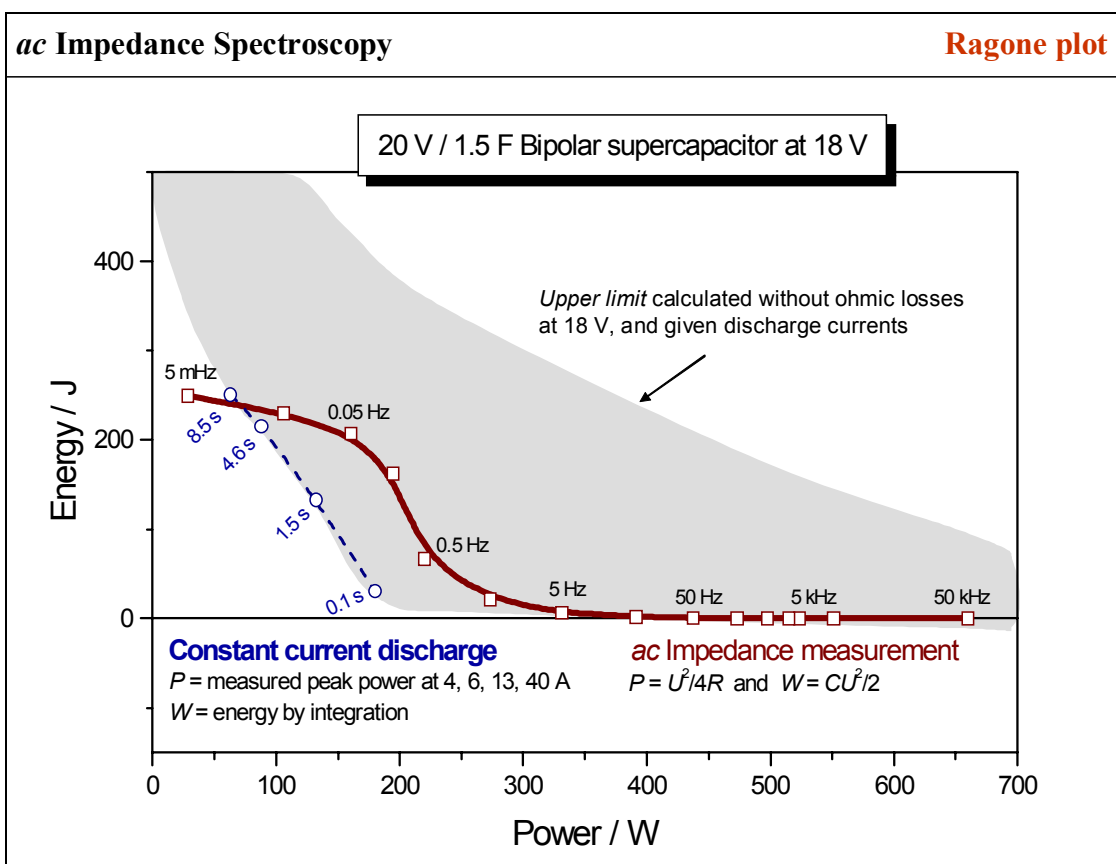
Herein $a = R_e S/(l A)$ is a constant depending on the pore resistance R_e , the surface roughness S/A . Constant b additionally depends on the double-layer and absorption capacitance, and the charge transfer resistance. The striking high-frequent quarter circle, and the low-frequency 45° slope in the complex plane plot occur with increasing surface roughness and pore resistance (constant a). Double-layer capacitor electrodes need therefore electrodes with optimized pore lengths and surface roughness.

ac Impedance Spectroscopy

Comparison with transient techniques



▲Fig.14



▲Fig.15

4.4 Aging tests based on the $C(R)$ diagram

The $C(R)$ diagram is excellently qualified to judge the aging and useful life of electrodes. Figure 17 shows lead dioxide coated on titanium. During electrolysis in sulfuric acid at high current densities, a poorly conducting interlayer grows between electrocatalyst and support. A second impedance arc forms at highest frequencies in the complex plane which is due to the interlayer impedance. Evidently, the $C(R)$ diagram reveals A1 with the highest capacitance as the most active electrode; A2 shows a lower capacitance, and B is useless due to the huge interlayer resistance of about 0.25Ω , which causes an enormous waste heat at high current densities.

Some few capacitance and resistance values gathered at a fixed frequency during a long-time experiment are sufficient to extrapolate the useful life of the electrode. The change of resistance $\Delta R/R$ reflects the growth of the interlayer, the change of capacitance $\Delta C/C$ the decline of electrochemical activity.

4.5 Chrono Impedance Spectroscopy – monitoring electrochemical aggregates in the $C(R)$ diagram

Chronological changes of capacitance and resistance in aging tests reflect deterioration and estimated life of the capacitor. The $C(R)$ diagram shows the best device left above at highest C and lowest R values.

Figure 18 shows the impedance spectra of a solid oxide fuel cell (SOFC) at different operating parameters. The $C(R)$ diagram helps to control and optimize temperature and gas flow rates. The best operating state 1 is found *at high capacitance and low resistance*, which corresponds to the left upper edge of the $C(R)$ diagram [17]. An insufficient hydrogen supply brings about the “bad” characteristics no. 3.

The high-frequent semicircle in the complex plane in Figure 18 describes the solid electrolyte made of zirconium dioxide stabilized with yttrium oxide. At medium frequencies the electrode reaction (charge transfer) is observed. The low-frequent semicircle reveals the gas supply. Thus, impedance spectroscopy qualifies for monitoring fuel cells and other electrochemical power sources without great effort.

In 2005, the European Space Agency (ESA) will launch an alkaline electrolyzer for oxygen and hydrogen production in space. The system will be monitored by chrono impedance spectroscopy. The method is described in [19].

The operation of chemical sensors using *ac* impedance spectroscopy is described in [21].

4.6 Design of electrode materials and electrolytes by help of the $C(R)$ diagram

Composite electrodes. In Figure 19, the $C(R)$ diagram reveals contact resistances more clearly than the complex plane plot. Activated carbon fibre cloth based on pitch (ACP), novoloid (ACN), and graphite (HMC) were coated on aluminium foils by means of thermoplastic binders. The best electrode is again situated at the left side in the $C(R)$ plot. The impedance spectra were measured at single capacitor cells consisting of two aluminium supported carbon fibre electrodes in a 1 molar solution of $[N(CH_2CH_3)_4]BF_4$ in acetonitrile.

Chemically modified carbon electrodes. Commercial carbon powders (such as VULCAN XC72R) were treated in concentrated aqueous acids and bases. One gram of carbon was immersed in an adequate volume of solution and heated in a reflux condenser for several hours. The products were separated from the solution by vacuum filtration. Finally, carbon pastes were produced by mixing the modified powders in a dispersion of PTFE in isopropanol. The paste was spread onto aluminium foils and dried at $90^\circ C$. Capacitor cells were built of two carbon paste electrodes and a polymer separator, soaked with $0,6 \text{ mol/l } [NEt_4]BF_4$ in acetonitrile.

Potassium hydroxide acts in a most favorable way on electrode capacitance, whereas concentrated sulfuric acid improves the interparticle resistance (Figure 20). Nitric acid destroys the carbon structure and causes the electrode resistance to rise. Further experiments are required to gain a full insight.

Electrolyte system. The $C(R)$ diagram helps to develop novel electrolytes (free of acetonitrile). Examples are given in [9].

Obscure electrode processes. The impedance spectrum reveals the mechanisms of charge storage, the contribution of the electrolyte resistance R_{el} , and the dielectric properties of the device. To further analyze the frequency response of capacitance and resistance, we suggest to evaluate the derivatives with respect to frequency. As both C and R are measured at the same frequencies, C may directly be differentiated to R . The dimension of the derivatives correlate again with Ohms and Farads.

$$\left[\frac{dC}{d\omega} \text{ or } \frac{dC}{dR} \cdot \frac{dR}{d\omega} \right] = \frac{F}{s^{-1}} = \frac{As^2}{V} = \frac{s^2}{\Omega}$$

$$\left[\frac{dZ}{d\omega} \right] = \frac{\Omega}{s^{-1}} = \frac{Vs}{A} = \frac{Vs^2}{C} = \frac{s^2}{F}$$

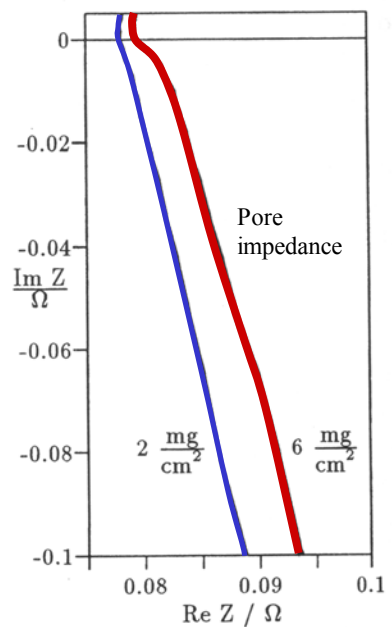
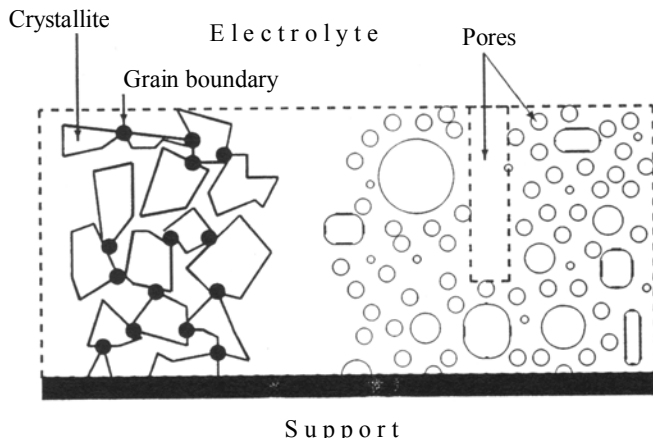
The method which we call *Derivative Impedance Spectroscopy* (DIS) is explained in [17].

ac Impedance Spectroscopy

Applications

Porous electrodes

Active metal oxide layer (compressed powder structure)

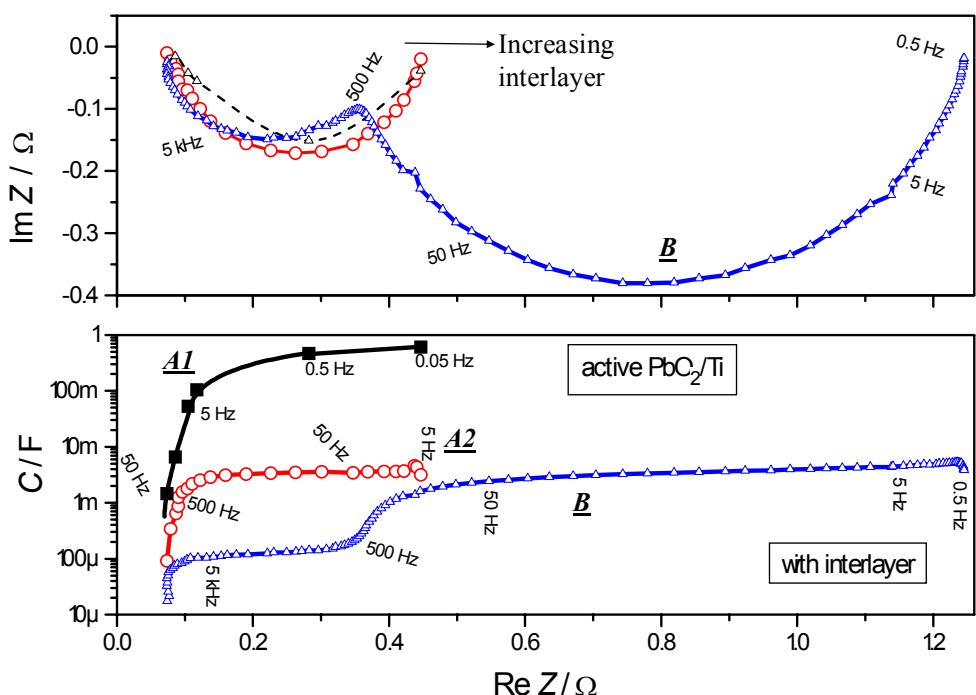
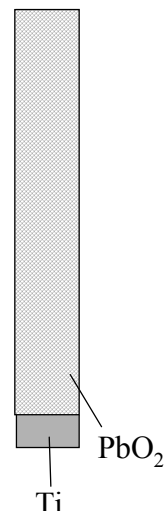


▲Fig.16

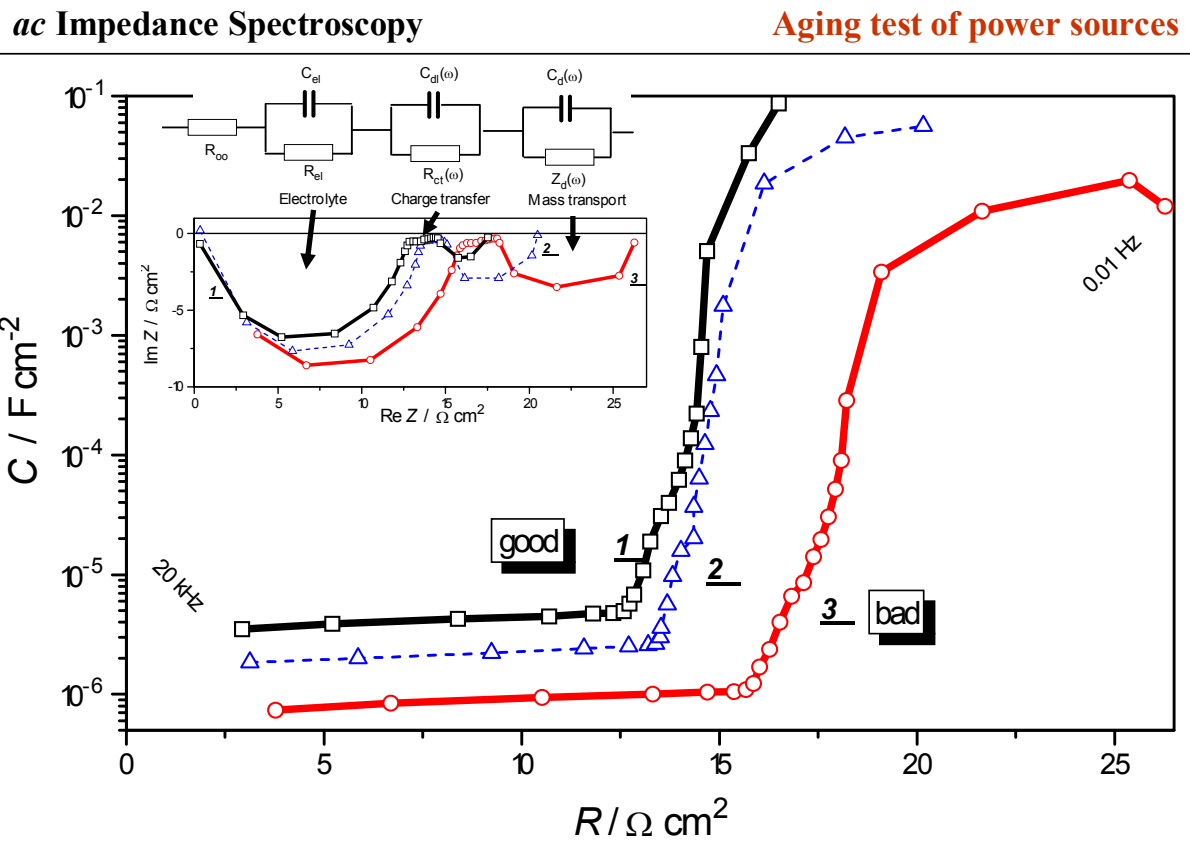
ac Impedance Spectroscopy

Applications

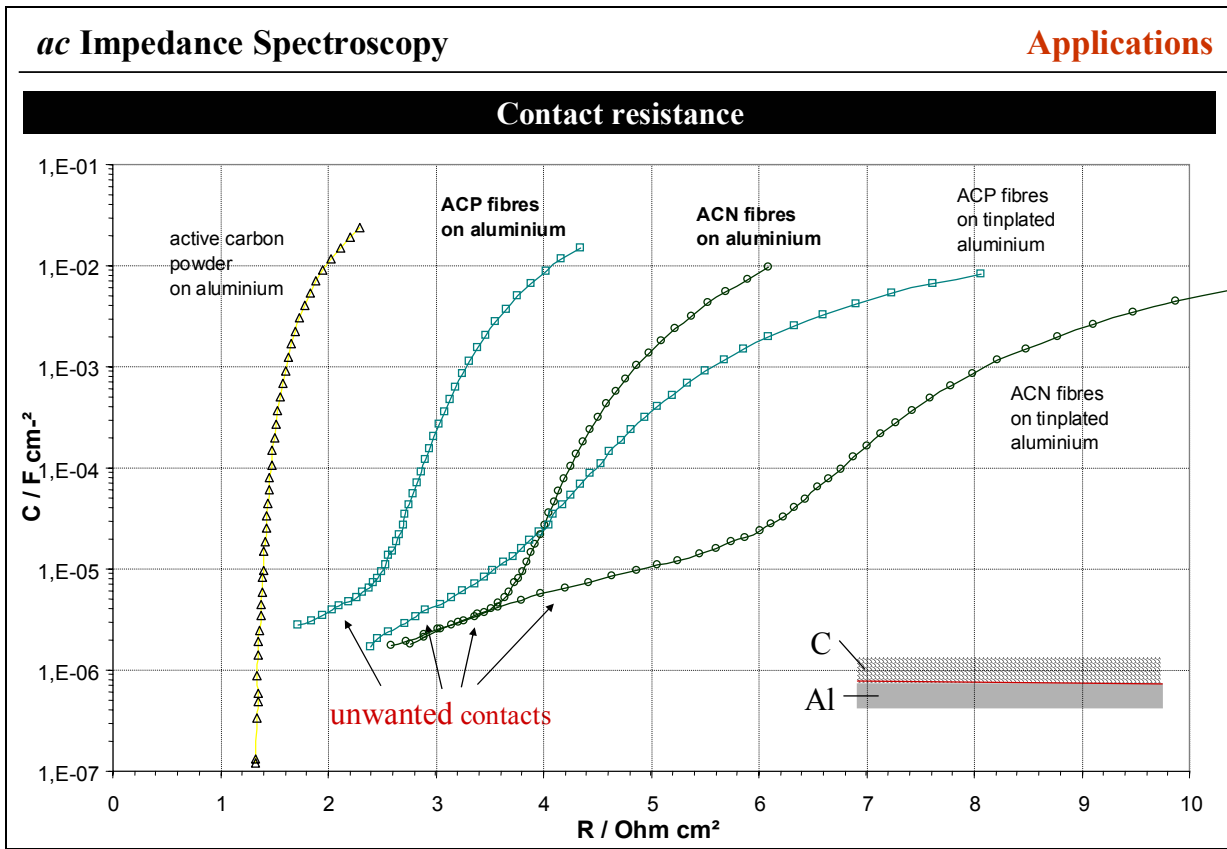
Aging test of lead dioxide electrodes



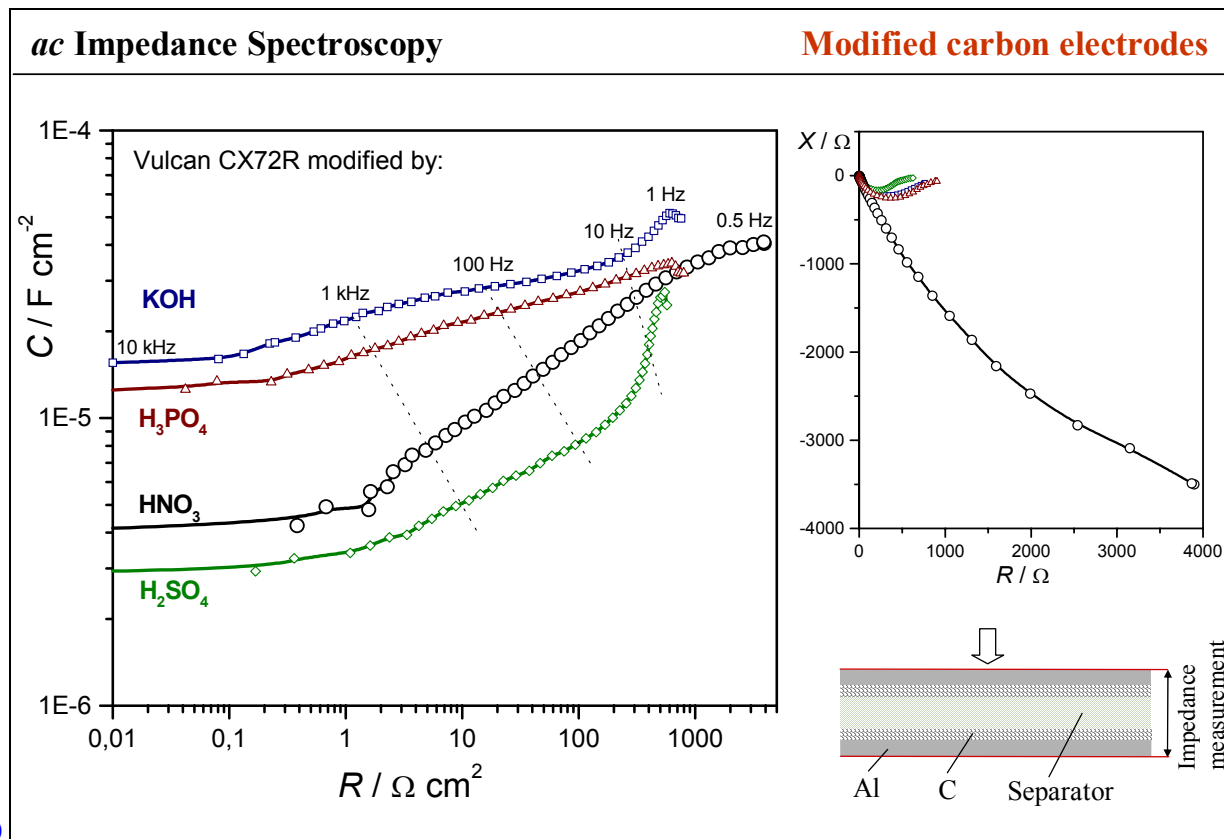
▲Fig.17



▲Fig.18



▲Fig.19



▲Fig.20

5. References

- [1] P. KURZWEIL, G. DIETRICH, Double-layer capacitors for energy storage devices in space applications, *Proc. 2nd Int. Seminar on Double Layer Capacitors*, Deerfield Beach, USA, Dec. 8-10, 1992.
- [2] S. TRASATTI, P. KURZWEIL, *Platinum Metals Review* **38** (1994) 46-56.
- [3] Double-layer capacitor, DE 43 13 474 A1 (1994); C2 (1997); DE 197 04 584 C2 (1999); US 5,930,108 (1999); EP 0 820 078 A1 (1998). Long time stable electrode, EP 0 622 815 B1 (1996). Electrode for an electrochemical cell, DE 196 40 926 C1 (1998).
- [4] P. KURZWEIL, O. SCHMID, High performance metal oxide supercapacitors, *Proc. 6th Int. Seminar on Double Layer Capacitors*, Deerfield Beach, USA, Dec. 9-11, 1996.
- [5] P. KURZWEIL, O. SCHMID, Low temperature proton conducting metal oxide supercapacitor, *Meeting Abstracts*, The Electrochem. Soc. Fall Meeting, San Antonio, Texas, October 6-11 (1996) 825.
- [6] P. KURZWEIL, O. SCHMID, A. LÖFFLER, Metal oxide supercapacitor for automotive applications, *Proc. 7th Int. Seminar on Double Layer Capacitors*, D. Beach, USA, Dec. 8-10, 1997.
- [7] P. KURZWEIL, H.-J. FISCHLE, Bipolar Supercapacitor For 42 V Applications, *Proc. 11th Int. Seminar on Double Layer Capacitors*, Deerfield Beach, USA, Dec. 3-5, 2001.
- [8] P. KURZWEIL, H.-J. FISCHLE, The HYDRA Supercapacitor – Energy storage based on carbon and mixed metal oxides, *Proc. 12th Int. Seminar on Double Layer Capacitors*, Deerfield Beach, USA, Dec. 9-11, 2002.
- [9] P. KURZWEIL, H.-J. FISCHLE, Double-Layer Capacitor Development And Manufacture By HYDRA/AEG, *Proc. 13th Int. Seminar on Double Layer Capacitors*, Deerfield Beach, USA, Dec. 8-10, 2003, pp. 1-11.
- [10] K. S. COLE, R. COLE, *J. chem. Phys.* **9** (1941) 341.
- [11] C. GABRIELLI, Identification of Electrochemical Processes by Frequency Response Analysis, The Solartron Electronic Group Ltd., Farnborough, UK (1980).
- [12] A. J. BARD, L. R. FAULKNER, *Electrochemical Methods*, John Wiley & Sons, New York 1980, Chapter 9.
- [13] A. HINTON, B. SAYERS, *Impedance Measurement Techniques: Sine Correlation*, Solartron, <http://www.solartronanalytical.com/technicalpages/techimped.html>, January 2004.
- [14] DIN IEC 62391-1, Fixed electric double layer capacitors for use in electronic equipment. Part I: Generic specification (IEC 40/1378/CD:2003), June 2004.
- [15] DIN IEC 62391-2, Fixed electric double layer capacitors for use in electronic equipment. Part I: Sectional specification: Electric double layer capacitors for power application (IEC 40/1379/CD:2003), June 2004.
- [16] H. W. SCHÜSSLER, *Networks, signals and systems* (in German), Vol. 1, Springer, Berlin 1988.
- [17] P. KURZWEIL, H.-J. FISCHLE, A new monitoring method for electrochemical aggregates by impedance spectroscopy, *J. Power Sources* **127** (2004) 331–340.
- [18] P. KURZWEIL, *German patent*, DE 102 20 172 A1 (2002).
- [19] P. KURZWEIL, J. OBER, D. W. WABNER, Method for extracting kinetic parameters from measured impedance spectra, *Electrochimica Acta* **34** (1989) 1179–1185.
- [20] R. DE LEVIE, in: *Advances in electrochemistry and electrochemical engineering*, ed: P. Delahay, C. T. Tobias, Vol. 6, p. 329, Interscience, New York 1967.
- [21] P. KURZWEIL, W. MAUNZ, C. PLOG, Impedance of zeolite-based gas sensors, *Sensors and Actuators B* **24–25** (1995) 653–656.

Acknowledgement. Discussions with Professor B. FRENZEL and the experiments of J. BRACKE and H. ROTHÄUGER are gratefully remarked.